Inorganic Chemistry

Article

pubs.acs.org/IC

Crystal Structures of Manganese and Cobalt Dichloride Monohydrate and Deuteration Effects on Magnetic Behavior

S. Pagola,*[,†] K. T. Trowell,[‡] K. C. Havas,[‡] Z. D. Reed,[‡] D. G. Chan,[‡] M. J. Van Dongen,[‡] and G. C. DeFotis*[,‡]

[†]Department of Applied Science and Applied Research Center and [‡]Department of Chemistry, College of William and Mary, Williamsburg, Virginia 23187-8795, United States

Supporting Information

ABSTRACT: This work reports the long sought crystal structures of the title members of the intriguing series of 3d transition metal dichloride monohydrates. The double chain structure which results from rearrangement of the well-known pseudo-octahedral coordination geometry and single chains in the corresponding metal chloride dihydrate is extremely unusual. $MnCl_2·H_2O$ and $CoCl_2·H_2O$ each crystallize in orthorhombic space group *Pnma* with $Z = 4$ and lattice parameters a = 9.0339(1), 8.8207(3); b = 3.68751(5), 3.5435(1); c = 11.5385(2), 11.2944(4) all in Å and for Mn, Co, respectively. Results are reported also for both fully deuterated systems; the structures remain the same with lattice parameter changes typically much less than 0.1%. Various magnetic properties of $MnCl_2·D_2O$ and $CoCl_2·D_2O$ are reported. For the latter, there are no apparent differences, qualitatively or quantitatively, from the previously measured properties of $CoCl_2·H_2O$. Interestingly, for the former some differences with respect to $MnCl_2·H_2O$ are apparent, principally a lower T_{max} = 3.10(10) K about which a broad antiferromagnetic maximum is centered, and a larger value χ_{max} = 0.336(3) emu/mol. However, antiferromagnetic ordering appears to occur at essentially the same 2.18(2) K. Results of fits to susceptibilities of $MnCl_2·D_2O$ and $CoCl_2·D_2O$ are compared with those obtained before for $MnCl_2·H_2O$ and $CoCl_2·H_2O$. Structural considerations serve to rationalize the physical properties, especially the lower dimensional magnetism of monohydrates.

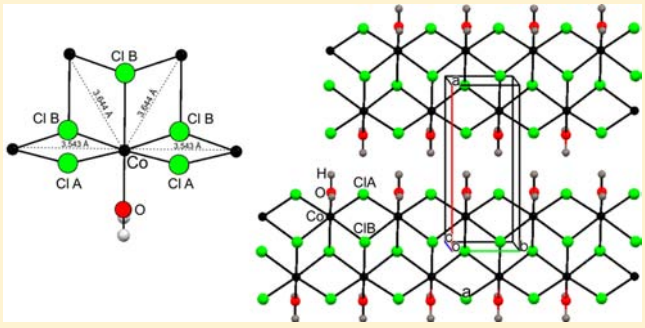

1. INTRODUCTION

The magnetic properties of the relatively unfamiliar monohydrate series of 3d transition metal dichlorides are quite interesting. Most thoroughly examined and remarkably contrasting are the Mn and Co systems, $MnCl_2·H_2O$ and $CoCl_2·H_2O$.[1−5] The magnetic susceptibilities and the heat capacities point to lower dimensional magnetism. This is in contrast to the three-dimensional magnetic lattice dimensionality of corresponding dihydrate materials.[6−8] However, while $MnCl_2·H_2O$ is a standard equilibrium magnetic system (as are all dihydrate materials irrespective of metal ion) $CoCl_2·H_2O$ displays pronounced nonequilibrium behavior.

The initial intent in preparing deuterated versions of the above two monohydrate systems was to facilitate possible neutron measurements. In most cases deuteration of hydrogen containing transition metal compounds leads to negligible effects on structural and magnetic properties. But this is not necessarily the case in systems like those here where waters coordinated to metal ions occur, especially if hydrogen bond pathways for exchange interactions are significant. This will be reviewed in detail in the final section.

However, of at least equal importance to the magnetic behaviors of deuterated forms of $MnCl_2·H_2O$ and $CoCl_2·H_2O$ reported here is the determination of the isomorphous crystal structures of these systems. A very unusual, probably unique, double chain structure is found. It is distinctly different from the simpler chloride bridged metal ion chains of the more extensively studied $MnCl_2·2H_2O$ and $CoCl_2·2H_2O$. Magnetic properties of corresponding (metal ion) dihydrate and monohydrate forms differ significantly, though some similarities also occur. Crystal structures of $MnCl_2·D_2O$ and $CoCl_2·D_2O$ are also determined and exhibit almost identical lattice constants as for $MnCl_2·H_2O$ and $CoCl_2·H_2O$. Yet, remarkably, while the magnetic properties of $CoCl_2·D_2O$ and $CoCl_2·H_2O$ are quantitatively indistinguishable, definite differences occur between those of $MnCl_2·D_2O$ and $MnCl_2·H_2O$. This finding, of evident interest but without clear explanation, is likely associated with an unexpected color difference as well. This may be the first report of such a contrast between D_2O and H_2O forms of a hydrated transition metal compound.

2. EXPERIMENTAL SECTION

Preparation of $MnCl_2·D_2O$ and $CoCl_2·D_2O$ proceeded along the lines described previously for H_2O containing materials. The major modifications were that fully deuterated D_2O (99.8%, Acros

Received: May 29, 2013
Published: November 19, 2013

   dx.doi.org/10.1021/ic4013075 | *Inorg. Chem.* 2013, 52, 13341−13350

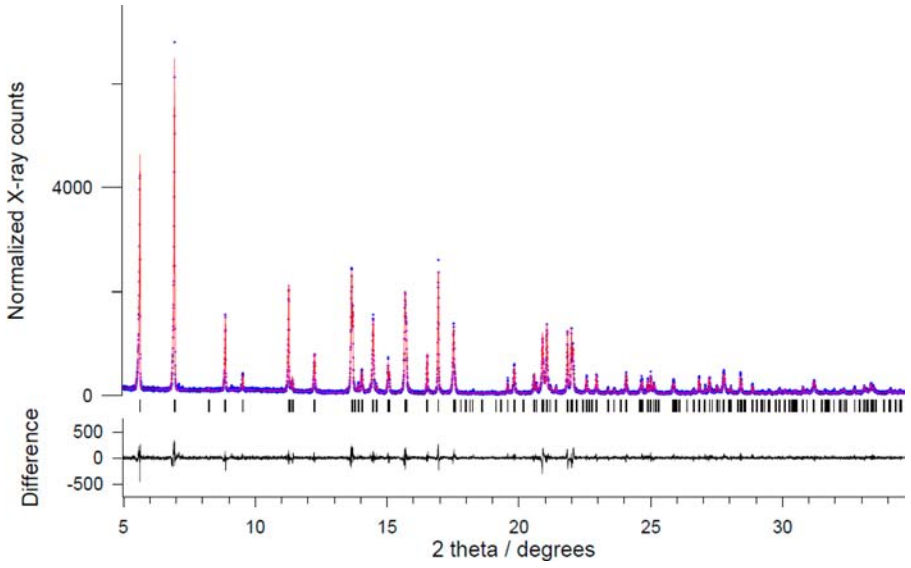

Figure 1. Rietveld refinement graph of $MnCl_2 \cdot H_2O$. Experimental powder diffraction intensities appear as dots, the calculated pattern as a solid line, with the difference between them at the bottom. Tick marks indicate allowed Bragg peak positions.

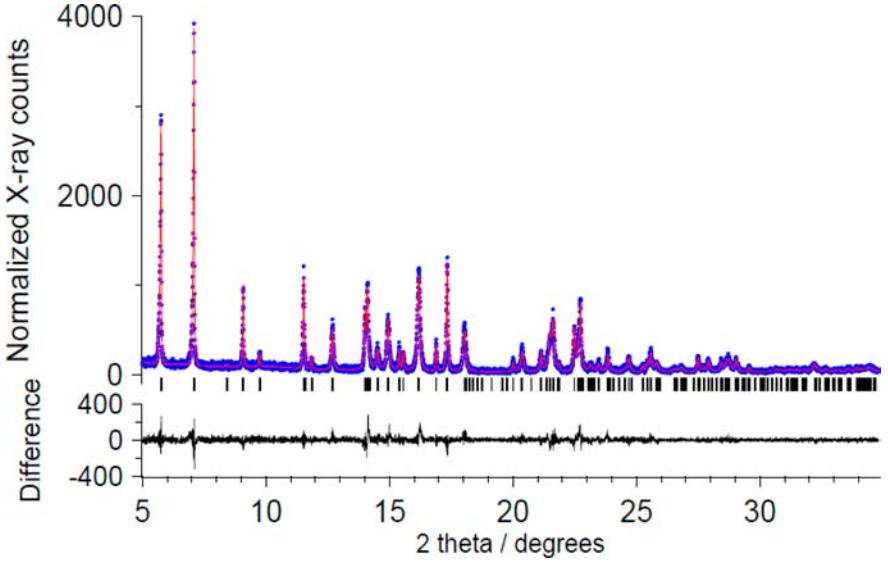

Figure 2. Rietveld refinement graph of $CoCl_2 \cdot H_2O$. Experimental powder diffraction intensities appear as dots, the calculated pattern as a solid line, with the difference between them at the bottom. Tick marks indicate allowed Bragg peak positions.

Chemicals) was employed as starting material along with high purity anhydrous metal dichloride, along with a vacuum oven and Ar(g) atmosphere while evaporating, to avoid exchange of D_2O with atmospheric water vapor. Temperatures similar to or slightly warmer than for the H_2O containing materials, 95 and 105 °C for manganese and cobalt systems, respectively, were found appropriate. The single D_2O hydration state of the fine polycrystalline material was confirmed by thermogravimetric analysis. No attempt by us or others to obtain a single crystal of any $MCl_2 \cdot H_2O$ system has been successful. An interesting color comparison emerges. $CoCl_2 \cdot D_2O$ is a blue-violet color as is $CoCl_2 \cdot H_2O$. However, while $MnCl_2 \cdot H_2O$ is a rather light pink, $MnCl_2 \cdot D_2O$ is a light gray-violet.

Magnetization and susceptibility measurements were made with a variable temperature vibrating sample magnetometer system. The data shown are field cooled measurements except where otherwise noted, and are corrected for the effects of diamagnetism and demagnetization, as well as the extremely small diamagnetism of the sample holder assembly. Polycrystalline samples of approximately 100 mg size were packed into nonmagnetic sample holders under dry conditions, weighed accurately, and then mounted in immediate proximity to a calibrated Cernox resistance thermometer. Temperatures are accurate to ±0.005−0.5 K depending on the range. Magnetic field values are accurate to ±max (2G, 0.1%), and magnetization and susceptibility data to 1.5% absolute, with a substantially better precision. Thus relative uncertainties in these quantities are within symbol size in plots appearing further on. In all handling of the materials care was taken to minimize exposure to atmospheric water vapor.

X-ray powder diffraction data for $MnCl_2 \cdot H_2O$ and $CoCl_2 \cdot H_2O$ were collected from 0.5 mm glass capillaries in the beamline X16C, Brookhaven National Laboratory at λ = 0.699204 Å. The wavelength was calibrated and the 2Θ zero error corrected using an Al_2O_3 flat plate NIST standard reference material. The wavelength was selected with a Si(111) double monochromator, and the incident parallel beam was monitored with an ion chamber. A Ge(111) analyzer crystal was placed after the sample and before the detector to increase the in-plane angular resolution, whereas the out-of-plane resolution was given by slits. A NaI(Tl) scintillation detector was used to measure the diffracted radiation. The diffraction data was collected at room temperature in the 2Θ interval 5°−35°, in 0.004° steps. The same

dx.doi.org/10.1021/ic4013075 | *Inorg. Chem.* 2013, 52, 13341−13350

procedure was subsequently employed for deuterated versions of both the Mn and the Co compounds.

3. CRYSTAL STRUCTURES

The X-ray powder diffraction patterns of $MnCl_2·H_2O$ and $CoCl_2·H_2O$ were indexed with the programs DICVOL[9] and TREOR,[10] respectively. The space group symmetry of $MnCl_2·H_2O$ was determined from the observation of the systematic absences from Le Bail fits of the patterns[11] carried out with the program FULLPROF,[12] and the International Tables for Crystallography.[13] Two space groups were possible, $Pbn2_1$ and *Pbnm*. The initial lattice parameters were permuted to use the standard setting of the space groups ($Pna2_1$, No.33 and *Pnma*, No. 62, respectively).

The crystal structure of $MnCl_2·H_2O$ was solved with the program EXPO2004,[14] using the direct methods optimized for the analysis of powder diffraction data. An analogous run for $CoCl_2·H_2O$ showed that this compound is isostructural with $MnCl_2·H_2O$. The Rietveld refinements[15] were carried out with the program GSAS.[16] The scale factor, background coefficients, lattice parameters, 2Θ zero error, absorption correction, pseudo-Voigt peak profile parameters[17] corrected by asymmetry,[18] atomic coordinates, and thermal displacement parameters were refined. The uncertainty in the atomic coordinates reported was corrected following Scott.[19]

Both compounds crystallize in the orthorhombic space group *Pnma* (No. 62) with $Z = 4$. The refined lattice parameters and cell volumes are as follows: $a = 9.0339(1)$ Å, $b = 3.68751(5)$ Å, $c = 11.5385(2)$ Å, $\alpha = \beta = \gamma = 90°$, $V = 384.38(1)$ Å^3 for $MnCl_2·H_2O$; and $a = 8.8207(3)$ Å, $b = 3.5435(1)$ Å, $c = 11.2944(4)$ Å, $\alpha = \beta = \gamma = 90°$, $V = 353.02(2)$ Å^3 for $CoCl_2·H_2O$. The results of the final Rietveld refinements are shown in the Figures 1 and 2. The agreement factors were $R_{wp} = 15.33\%$, $\chi^2 = 1.284$, $R_I = 4.92\%$ for $MnCl_2·H_2O$; and $R_{wp} = 16.65\%$, $\chi^2 = 1.238$, $R_I = 3.86\%$ for $CoCl_2·H_2O$. Here R_I is the R-Bragg factor defined in standard texts,[15b] as are the other quantities listed. Less ideal crystallinity of the cobalt sample is responsible for the broader peaks than in the manganese compound.

Very similar data collection and analysis was subsequently carried out on the fully deuterated forms of the same two compounds. The deuterated compounds are isostructural. The previously refined atomic coordinates of the hydrogenated compounds were used as the starting model for the Rietveld fits of the deuterated structures. The refined lattice parameters and cell volumes are as follows: $a = 9.0345(2)$ Å, $b = 3.68721(8)$ Å, $c = 11.5356(3)$ Å, $\alpha = \beta = \gamma = 90°$, $V = 384.28(2)$ Å^3 for $MnCl_2·D_2O$; and $a = 8.8258(2)$ Å, $b = 3.5446(1)$ Å, $c = 11.2998(4)$ Å, $\alpha = \beta = \gamma = 90°$, $V = 353.50(2)$ Å^3 for $CoCl_2·D_2O$. The agreement factors were $R_{wp} = 17.32\%$, $\chi^2 = 1.221$, $R_I = 4.73\%$ for $MnCl_2·D_2O$; and $R_{wp} = 20.76\%$, $\chi^2 = 1.371$, $R_I = 5.18\%$ for $CoCl_2·D_2O$.

The fractional atomic coordinates and isotropic thermal displacement parameters are shown in the Tables 1 and 2, respectively. Additional crystallographic information is summarized in the Supporting Information (cif) files.

The crystal structure of $MnCl_2·H_2O$ is composed of hydrogen bonded infinite double chains of edge-sharing $MnCl_5O$ octahedra extending along the *b*-axis. Figure 3 shows the structure down [010], depicting the cross-sectional view of the double chains and the hydrogen bonding pattern viewed along this direction.

As a rule, the atomic coordinates of hydrogen atoms cannot be determined from X-ray powder diffraction patterns. For the present compounds, the H positions were calculated to produce suitable H-bonding geometries, and they were included in the Rietveld refinements (additional details of the refinements are in the cif files). Considering the Cl−O interatomic distances so determined, one concludes that each double chain is hydrogen bonded to six other double chains in the crystal structure (see Figure 3), with ClA−O shortest distances of 3.282(28) and 3.256(28) Å. ClB−O is larger, 3.632(24) Å. The interchain hydrogen bonding happens at multiple water positions along [010], and this can be seen in Figure 4, a view of the structure approximately down the [001] direction.

Each octahedron of an individual strand of the double chain shares four edges with four adjacent octahedra, two of those along the same strand, and another two in the remaining strand of the double chain. The arrangement so formed is also represented in Figure 4. The octahedra are slightly distorted. The relevant bond lengths in this discussion are summarized in Table 3. Each chloride ion labeled ClA is bonded to two Mn(II) ions with Mn−ClA distances of 2.500(9) Å each, and is hydrogen bonded to two water molecules with ClA−O distances of 3.256(28) and 3.282(28) Å (represented in Figure

Table 1. Fractional Atomic Coordinates and Isotropic Thermal Displacement Parameters of $MnCl_2·H_2O$ and (Bottom Half) $MnCl_2·D_2O$[a]

site	*x*	*y*	*z*	U_{eq} (Å^2)
Mn	0.1831(9)	0.25	0.4815(7)	0.0183(2)
ClA	0.310(1)	−0.25	0.589(1)	0.028(5)
ClB	0.035(2)	−0.25	0.375(1)	0.020(5)
O	0.336(3)	0.25	0.347(2)	0.08(1)
H	0.3140	0.25	0.2655	0.092
H	0.4425	0.25	0.3499	0.092
Mn	0.18315(79)	0.25	0.48155(61)	0.0174(30)
ClA	0.3106(12)	−0.25	0.5885(10)	0.0250(46)
ClB	0.0345(12)	−0.25	0.3745(10)	0.0180(41)
O	0.3377(28)	0.25	0.3474(20)	0.063(10)
D	0.3152	0.25	0.2662	0.076
D	0.4437	0.25	0.3507	0.076

[a]The numbers in parentheses are the estimated uncertainties in the last significant digits. All atoms are in the Wyckoff position 4c.

Table 2. Fractional Atomic Coordinates and Isotropic Thermal Displacement Parameters of $CoCl_2·H_2O$ and (Bottom Half) $CoCl_2·D_2O$[a]

site	*x*	*y*	*z*	U_{eq} (Å^2)
Co	0.179(1)	0.25	0.4818(8)	0.012(4)
ClA	0.307(2)	−0.25	0.592(2)	0.024(7)
ClB	−0.033(2)	0.25	0.626(2)	0.014(6)
O	0.334(4)	0.25	0.352(3)	0.04(2)
H	0.3110	0.25	0.2687	0.048
H	0.4426	0.25	0.3549	0.048
Co	0.17866(98)	0.25	0.48132(76)	0.0099(33)
ClA	0.3087(18)	−0.25	0.5870(15)	0.0182(61)
ClB	−0.0331(18)	0.25	0.6238(12)	0.0119(58)
O	0.3314(36)	0.25	0.3532(27)	0.050(15)
D	0.3085	0.25	0.2703	0.061
D	0.4400	0.25	0.3565	0.061

[a]The numbers in parentheses are the estimated uncertainties in the last significant digits. All atoms are in the Wyckoff position 4c.

dx.doi.org/10.1021/ic4013075 | *Inorg. Chem.* 2013, 52, 13341−13350

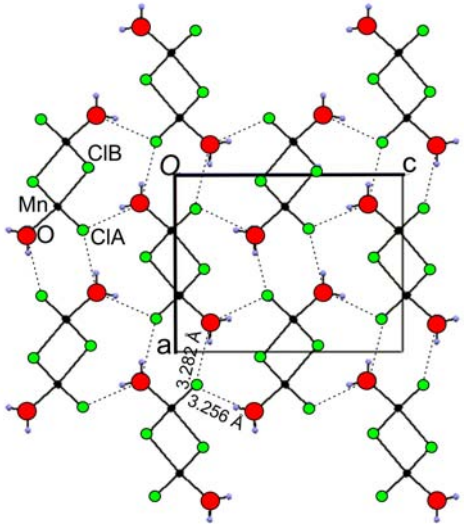

Figure 3. Crystal structure of $MnCl_2·H_2O$ viewed down [010]. Mn atoms are small black spheres, Cl medium green spheres, O large red spheres, and H small spheres. Atom sizes are shown at 50% probability level. Cl−O hydrogen bonds are indicated by dashed lines; the two shortest such distances (ClA−O) are shown.

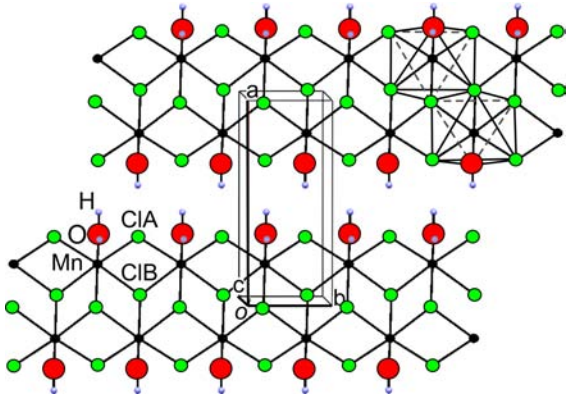

Figure 4. Crystal structure of $MnCl_2·H_2O$ viewed approximately down [001]. Mn atoms are small black spheres, Cl medium green spheres, O large red spheres, and H small spheres. Atom sizes are shown at 50% probability level. Two $MnCl_5O$ octahedral sharing edges are outlined.

3). The ClB ion is bonded to three Mn(II) ions. Two of the Mn−ClB bond distances are 2.588(12) Å each, and the remaining one (running approximately in opposite direction to the Mn−O bond) is 2.574(18) Å. The Mn−O distance is 2.08(3) Å. A local view of the peculiar double chain coordination geometry, with relevant Mn−Mn distances, appears in Figure 5.

An analogous analysis is valid for $CoCl_2·H_2O$, and the corresponding bond lengths are shown in Table 3. The two intradouble chain Mn−Mn distances are 3.688 and 3.812 Å. For the Co compound these are 3.543 and 3.644 Å, respectively.

Numerical values and comparisons in the last paragraphs are for H-containing materials. Atomic positions for D-containing materials in Tables 1 and 2 are extremely similar to those of the former. The lattice constants on going from H to D change by less than 0.1% in all cases, usually by much less. Quite small also are variations in bond lengths, Table 3, from H to D forms. For the two manganese systems variations are in general 0.01 Å or less, and appear to occur randomly in either direction. For

Table 3. Selected Bond Lengths (in Å) in $MnCl_2·H_2O$ and $CoCl_2·H_2O$ (Top Half) and $MnCl_2·D_2O$ and $CoCl_2·D_2O$ (Bottom Half)[a]

$MnCl_2·H_2O$		$CoCl_2·H_2O$	
Mn−ClA	2.500(9) × 2	Co−ClA	2.442(15) × 2
Mn−ClB	2.588(12) × 2	Co−ClB	2.506(15) × 2
Mn−ClB	2.574(18)	Co−ClB	2.48(2)
Mn−O	2.08(3)	Co−O	2.01(4)
O−ClA	3.282(28)	O−ClA	3.189(41)
O−ClA	3.256(28)	O−ClA	3.229(39)
O−ClB	3.632(24)	O−ClB	3.569(35)
$MnCl_2·D_2O$		$CoCl_2·D_2O$	
Mn−ClA	2.499(9) × 2	Co−ClA	2.426(13) × 2
Mn−ClB	2.594(9) × 2	Co−ClB	2.491(12) × 2
Mn−ClB	2.574(13)	Co−ClB	2.467(17)
Mn−O	2.09(3)	Co−O	1.98(4)
O−ClA	3.273(26)	O−ClA	3.247(35)
O−ClA	3.262(27)	O−ClA	3.252(35)
O−ClB	3.621(23)	O−ClB	3.610(30)

[a]Numbers in parentheses are estimated uncertainties in the last significant digits.

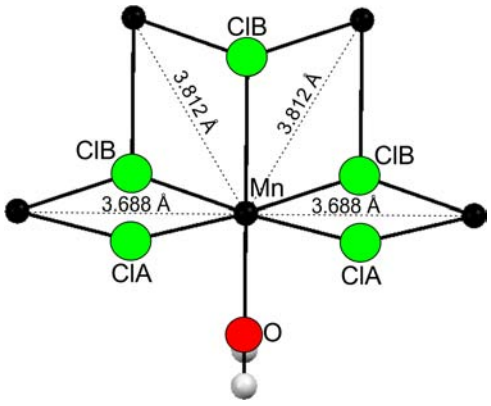

Figure 5. Local view of double chain coordination geometry in $MnCl_2·H_2O$, with smallest and next smallest Mn−Mn separations indicated.

the cobalt materials bond length variations can be somewhat larger, most evident in O−Cl separations. Even so, the 0.02−0.05 Å larger values for $CoCl_2·D_2O$ are not beyond mutual experimental uncertainties. It is unlikely that any significant structural variation is implied.

4. MAGNETIC MEASUREMENTS

A. Magnetic Susceptibility. *i. Moderate to High Temperature Data.* Figure 6 shows the inverse molar magnetic susceptibilities vs temperature for the two deuterated materials examined here. A Curie−Weiss form fit, $\chi_M = C/(T - \Theta)$ to the $MnCl_2·D_2O$ data, between 30 and 300 K (as previously for $MnCl_2·H_2O$) yields C = 4.38(2) emu K/mol and Θ = −8.6(4) K. From the standard Curie constant expression and S = 5/2, a g value of 2.005(5) results, very much as expected for isotropic Mn(II). The Θ value is somewhat more negative than that found previously for $MnCl_2·H_2O$, −4.9 K.[1] It remains, however, substantially smaller in magnitude than the −14.5 K of $MnCl_2·2H_2O$.[20] These results for $MnCl_2·D_2O$ along with others obtained in section A.ii. appear in Table 4, together with previous results for $MnCl_2·H_2O$ for comparison purposes.

In contrast, over no significant moderate to high temperature range is the inverse susceptibility of $CoCl_2·D_2O$ linear, very

dx.doi.org/10.1021/ic4013075 | Inorg. Chem. 2013, 52, 13341−13350

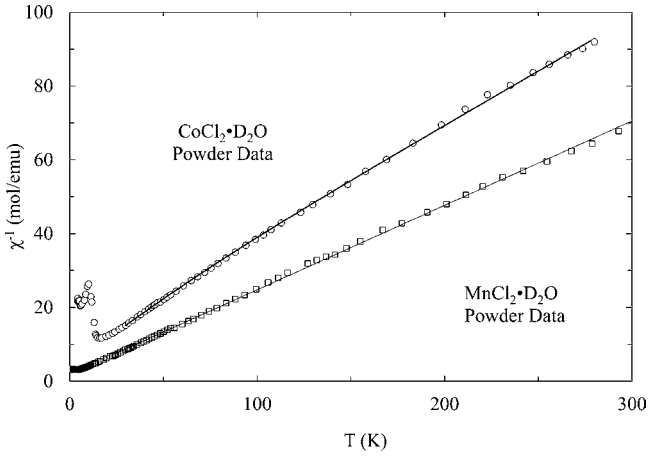

Figure 6. Inverse molar magnetic susceptibilities vs temperature for $MnCl_2 \cdot D_2O$ and $CoCl_2 \cdot D_2O$. A Curie−Weiss fit to the former, described in text, appears as a straight line through the squares. A curve corresponding to a ground and excited Kramers doublet fit, with a mean-field accounting for exchange interactions, described in the text, appears through the circles. For clarity the cobalt compound results have been shifted up 10 mol/emu.

much as had also been so for the H_2O containing material. If one fits the restricted but plausibly linear 29−70 K region as for $CoCl_2 \cdot H_2O$ previously there result C = 2.94(2) emu K/mol and Θ = 14.4(4) K. These are only 0.05 emu K/mol (1.7%) and 0.4 K (2.7%) lower than values for the H_2O containing material. As there the Θ value in particular is much more positive than the value measured in this laboratory for $CoCl_2 \cdot 2H_2O$, −7.5 K.[20] These results for $CoCl_2 \cdot D_2O$ along with others obtained in the following paragraphs appear in Table 5, together with previous results for $CoCl_2 \cdot H_2O$ for comparison purposes.

For weak octahedral coordination the crystal field ground term of Co(II) is a $^4T_{1g}$ level. Crystal field distortions and spin−orbit coupling split this level into six Kramers doublets. Curie(−Weiss) behavior is expected if only the ground doublet is significantly populated over the accessible temperature range. This was found previously not to be the case for $CoCl_2 \cdot H_2O$, as it appears not to be here. Hence we adopt a similar approach and account for the $CoCl_2 \cdot D_2O$ data assuming that the first excited doublet is a moderate ΔE above the ground Kramers doublet, but that more excited doublets are so much higher in energy as to make negligible contribution to the observed susceptibility. Allowance is made for different g values, g_1 and g_2, characterizing the ground and excited doublets. The Van Vleck equation[21a] applied to this situation, treating each of the two doublets as an effective $S' = 1/2$, yields

$$\chi = 0.0938 \frac{g_1^2 + g_2^2 e^{-\Delta E/kT}}{T(1 + e^{-\Delta E/kT})} \quad (1)$$

where the numerical prefactor has dimensions emu K/mol. Exchange interactions, obviously present and substantial, are accounted for in a mean-field approximation, employing the expression

$$\chi_{ex} = \chi/[1 - (2zJ/N_0 g^2 \mu_B^2)\chi] \quad (2)$$

where J is a mean interaction over z neighbors.[21b]

Susceptibility data for $CoCl_2 \cdot D_2O$ were fit in the 30−300 K range employing eqs 1 and 2. The fitted curve appears in Figure 6 along with the data. Optimal parameter values are g_1 = 5.44, g_2 = 6.57, $\Delta E/k$ = 230 K, and zJ/k = 31.2 K. These appear in Table 5 along with values obtained for $CoCl_2 \cdot H_2O$ previously.[4] The rms deviation for the fit is 1.2%, even slightly better than the 1.5% for $CoCl_2 \cdot H_2O$ previously. The quality of fit and parameter values are quite similar for the two compounds. The nearly identical outcome is reinforced indirectly by the virtually indistinguishable character of the lower temperature susceptibility discussed in section A.ii.

This approach to fitting the data is phenomenological. Calculations involving multiparameter ligand field models, even with idealized assumptions such as tetragonal symmetry, are extremely difficult to do reliably;[22] but see the next paragraph. The local coordination geometry here in conjunction with the double chain structure is not close to such a description. The individual Kramers doublets are variably anisotropic depending on detailed distortions, energy separations, and other parameters. This provides some rationalization for the large fitted g values, pronouncedly Ising like, of both ground and first excited doublet. That the model fits the data quite well over a rather broad temperature range, and involves a plausible minimum number of parameters, can be considered significant. No comparable fit was obtained with rather different g_1, g_2, and ΔE. The mean field exchange inferred is consistent (within 8%) with the low temperature Θ(obs) via the mean-field relation $\Theta = 2S(S + 1)zJ/3k$. It is also small compared to ΔE.

An alternative attempt was made, but unsuccessful, to compare our results with those of ref 22. The effective magnetic moment was calculated from the standard formula $\mu_{eff} = 2.828[\chi_M T]^{1/2}$ in Bohr magnetons, and also employing a sometimes seen alternative expression with T replaced by $(T - \Theta)$, substituting Θ = 14.4 K from the limited linear regime fit noted earlier. All d^7 diagrams of ref 22, representing a wide range of combinations of site symmetry, spin−orbit coupling, orbital reduction factor, and ligand field strength, were checked. Not even approximate agreements were found when insisting that the ligand field strength should yield a colored compound.

ii. Low to Moderate Temperature Data. Magnetic susceptibility data for $MnCl_2 \cdot D_2O$ below 40 K appear in Figure 7, obtained in fields of 100 or 200 G depending on the temperature, as for $MnCl_2 \cdot H_2O$ previously.[1] In principle a zero-field splitting of a sextet Mn(II) crystal field ground term can yield a maximum in $\chi(T)$, χ_{max}, at temperature T_{max}. However energy parameters D, in a $D[\hat{S}_z^2 - S(S + 1)/3]$ spin Hamiltonian, are for Mn(II) compounds typically of order several 0.01 K, and rarely exceed a few 0.1 K. The consequent 6|D| zero-field splitting is such as to yield a χ_{max} only at much lower temperature than the 3−4 K here, assuming no

Table 4. Magnetic Parameters for $MnCl_2 \cdot D_2O$ and $MnCl_2 \cdot H_2O$ Data and Fits[a]

system	C (emu K/mol)	Θ (K)	T_{max} (K)	χ_{max} (emu/mol)	J/k (K)	$z'J'/k$ (K)
D_2O	4.38(4)	−8.6(4)	3.10(10)	0.336(3)	−0.374(5)	−0.08(2)
H_2O	4.25(5)	−4.9(3)	3.60(10)	0.304(3)	−0.493(5)	−0.06(2)

[a]Numbers in parentheses are estimated uncertainties in the last significant digits.

dx.doi.org/10.1021/ic4013075 | Inorg. Chem. 2013, 52, 13341−13350

Table 5. Magnetic Parameters for $CoCl_2 \cdot D_2O$ and $CoCl_2 \cdot H_2O$ Data and Fits[a]

system	C (emu K/mol)	Θ (K)	T_{max} (K)	χ_{max} (emu/mol)	$\Delta E/k$ (K)	g_1 g_2	zJ/k (K)
D_2O	2.94(2)	14.4(4)	16.2(2)	0.615(5)	230(15)	5.44(5) 6.57(5)	31.2(5)
H_2O	2.99(2)	14.8(3)	16.2(2)	0.604(5)	230(10)	5.51(3) 6.66(5)	32.5(3)

[a]Numbers in parentheses are estimated uncertainties in the last significant digits.

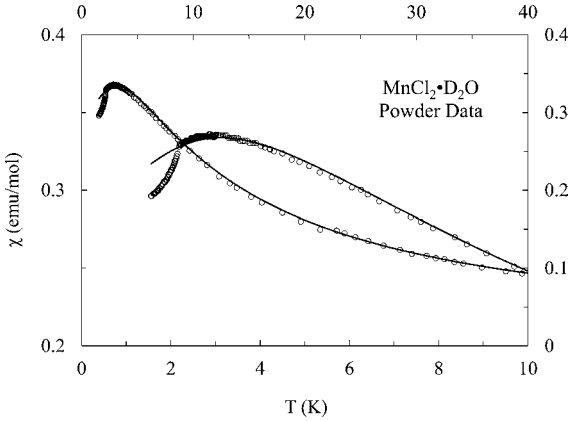

Figure 7. Molar magnetic susceptibility versus temperature for $MnCl_2 \cdot D_2O$. Left and bottom axes are for 0 to 10 K representation; right and top axes for 0 to 40 K. Curves through data are according to a classical one-dimensional spin-5/2 Heisenberg model with interchain exchange, described in the text.

antiferromagnetic ordering has occurred.[21a] Moreover, in the present case the sharp drop in $\chi(T)$ at 2.18 K is not a feature that zero-field splitting effects can cause.

Therefore, the susceptibility maximum for $MnCl_2 \cdot D_2O$ is attributed to antiferromagnetic interactions, and as for $MnCl_2 \cdot H_2O$ previously[1] of a low dimensional nature given the broadness of the maximum. Hence, also shown in Figure 7 is the optimal fit obtained employing a classical one-dimensional Heisenberg model scaled to spin $S = 5/2$. Before describing the fit one should note certain straightforward comparisons between these data and those of the H_2O containing material. As there a sharp drop in the susceptibility occurs at a temperature somewhat lower than that of the maximum. However, the location of the maximum is significantly shifted here, being at 3.10(10) K vs 3.60(10) K in $MnCl_2 \cdot H_2O$. The size of the maximum is also different, 0.336(3) emu/mol here vs 0.304(3) emu/mol in $MnCl_2 \cdot H_2O$. An antiferromagnetic maximum at lower temperature corresponds to a weaker exchange interaction which leads to a larger susceptibility value at the maximum. Despite these differences the apparent transition temperature T_c, signaled by a maximum $d\chi/dt$ on the low temperature side of the maximum, is virtually unchanged (within 0.01−0.02 K) from its location in $MnCl_2 \cdot H_2O$ and is at 2.18(2) K. Hence there is a difference in the characteristic T_c/T_{max} ratio: 0.70 here versus 0.60 in $MnCl_2 \cdot H_2O$. However, both are very much below the ≥0.9 values which obtain for three-dimensional magnets.

The classical (which should serve well for large $S = 5/2$) one-dimensional Heisenberg model expression is[23]

$$\chi = [N_0 g^2 \mu_B{}^2 S(S+1)/3kT][(1-u)/(1+u)] \qquad (3)$$

where $u = T/T_0 - \coth(T_0/T)$ and $T_0 = 2JS(S+1)/k$ and the exchange interaction convention employed is $-2J\sum_{i>j}\hat{S}_i \cdot \hat{S}_j$. Interchain exchange is taken into account via a mean field correction expression of the same form as eq 2 except that now reference is made to z' and J' for the effective number of interchain neighbors and the corresponding interaction. This is the same fitting procedure as applied to $MnCl_2 \cdot H_2O$ previously. The data are fit between 2.4 and 40 K, and the resulting parameter values are $g = 2.00$, $J/k = -0.37_4$ K and $z'J'/k = -0.38$ K, each a percent or so uncertain. The rms deviation for the fit is 0.81%, comparable with though not quite so good as the 0.63% for $MnCl_2 \cdot H_2O$ previously.[1] The g value agrees with that of the Curie−Weiss fit in the high temperature range, while the J/k value positions the calculated susceptibility maximum quite close to where it actually appears. The fitted curve appears in Figure 7 in both a 0 to 40 K and a finer 0 to 10 K representation. A plausible number of interchain neighbors is $z' = 4$ (this is also assumed in the theory discussed below), whence $J'/k = -0.095$ K. This is substantially smaller (25%) than the main intrachain exchange interaction but also somewhat larger in relation to it than was a similarly obtained estimate in $MnCl_2 \cdot H_2O$.

No magnetic phase transition at any temperature is predicted for the purely one-dimensional Heisenberg model. But interchain exchange can induce a transition. Thus a more reliable estimate of the latter can be obtained based on the observed T_c. The same first order and second order Green's function theory expressions applied previously in the case of $MnCl_2 \cdot H_2O$ will be used here.[24−26] The input is the transition temperature 2.18 K, the estimated intrachain exchange $J/k = -0.37_4$ K, and also the spin value 5/2. From first order theory one estimates that $\eta = |J'/J|$, the ratio of interchain to intrachain interaction magnitudes, is 0.10_2. Hence $|J'/k| = 0.038$ K and is almost certainly negative, because a classical model generally yields a too strong antiferromagnetic exchange, suggesting that some antiferromagnetic interaction should be associated with interchain exchange. From second order theory one estimates that $|J'/k| = 0.0104$ K, again almost certainly negative. Since first and second order results tend to overestimate and underestimate respectively, the interchain exchange, and by about the same factor for $S = 5/2$, we will take as most plausible the geometric mean of these results, which is $J'/k = (-)0.020$ K. This is definitely of smaller size than the estimate provided by the mean field correction in the one-dimensional model fit. With $z' = 4$ assumed in the theory this is the value entered in Table 4.

The magnetic susceptibility of $CoCl_2 \cdot D_2O$ below 30 K appears in Figure 8, obtained in a 200 G applied field as for $CoCl_2 \cdot H_2O$ previously.[3] The position of the susceptibility maximum is the same $T_{max} = 16.2(2)$ K as for $CoCl_2 \cdot H_2O$. The size of the susceptibility at the maximum is $\chi_{max} = 0.615(5)$ emu/mol, only 1−2% larger than the 0.604 emu/mol in $CoCl_2 \cdot H_2O$, which is not considered significant. It is noteworthy that such χ_{max} are approximately three times larger than observed[8,20] for $CoCl_2 \cdot 2H_2O$ with a T_{max} only 8% higher. The atypical size and shape of χ_{max} renders unreliable an inflection based estimate of T_c. From the virtual identity of the observed susceptibility with that of $CoCl_2 \cdot H_2O$ it is very probable that the same $T_c = 15.0$ K obtains.

dx.doi.org/10.1021/ic4013075 | Inorg. Chem. 2013, 52, 13341−13350

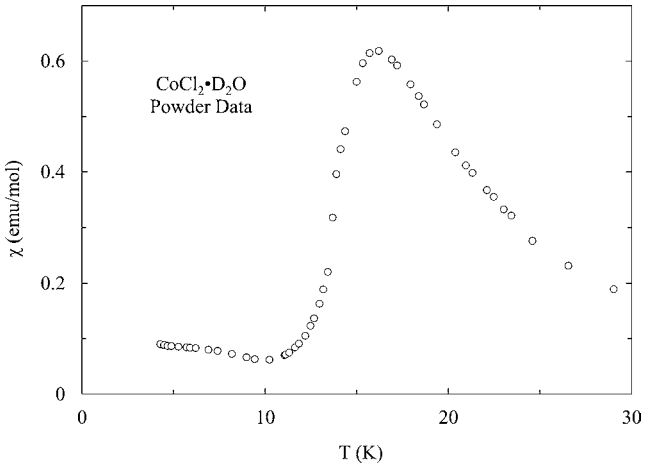

Figure 8. Molar magnetic susceptibility below 30 K of $CoCl_2 \cdot D_2O$.

The very large χ_{max} results from the strong net ferromagnetic exchange interaction, as reflected in Table 5 parameters already noted. Therefore, despite the appearance of a susceptibility maximum, the data cannot be fit (in contrast to the manganese compounds) by any plausible model, for example, one-, two- or three-dimensional Ising antiferromagnet, as often works for Co(II) materials. Many attempts to do so failed, even with interchain or interlayer interactions incorporated via eq 2, and allowing for different sign combinations of primary and secondary interactions. T_{max} and χ_{max} values are inconsistent in the context of such models.

B. Magnetization. Figure 9 shows isotherms for $MnCl_2 \cdot D_2O$. Hysteresis is essentially negligible at all temperatures. For

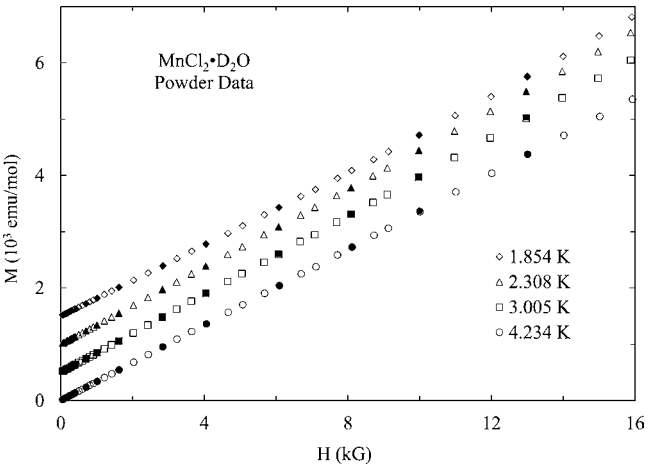

Figure 9. Isothermal molar magnetization vs field for $MnCl_2 \cdot D_2O$ at various temperatures. For clarity successively lower temperature isotherms are shifted up 500, 1000, and 1500 emu/mol. Solid symbols are on decreasing field from 16 kG. The last digit in the temperatures is more uncertain (±3) than others but still estimatable.

the two higher ones, well above the estimated transition at 2.18 K, excellent linearity is present at all fields. At 2.308 K, and decidedly more so at 1.854 K, below the transition, convex upward curvature is detectable. It is plausible that a spin flop transition occurs at substantially higher field and that its early onset is responsible for the curvature observed. $MnCl_2 \cdot H_2O$ was not examined in the same detail, but a 1.84 K isotherm (also below the virtually identical 2.18 K transition there, and with very comparable T/T_c ratio) displayed similar curvature. However, in the case of the H_2O containing material the departure from linearity over the same field range was about twice as large.

Figure 10 shows isothermal magnetization data for $CoCl_2 \cdot D_2O$. The behavior is much more complicated than for the

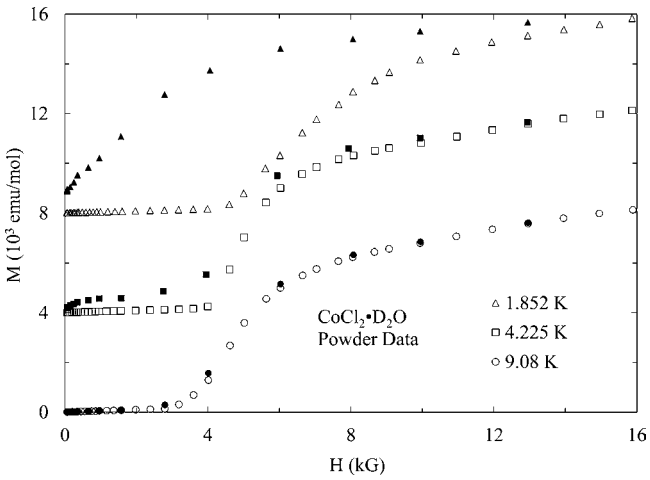

Figure 10. Isothermal molar magnetization vs field for $CoCl_2 \cdot D_2O$ at various temperatures. For clarity successively lower temperature isotherms are shifted up 4000 and 8000 emu/mol. Solid symbols are on decreasing field from 16 kG. The last digit in the temperatures is more uncertain (±3) than others but still estimatable.

manganese compound, with clear field induced transitions visible and enormously enhanced hysteresis as the temperature is lowered. Comparison with previously published data[5] for $CoCl_2 \cdot H_2O$ shows essentially identical behavior, both qualitatively and quantitatively. Although it was not feasible here (for instrumental reasons) to examine the field cooled and zero-field cooled magnetization in comparable detail as for $CoCl_2 \cdot H_2O$ previously, less extensive measurements revealed the same kind and degree of difference between these quantities, and hence very similar irreversibility.

Data have been obtained for $MnCl_2 \cdot D_2O$ and $MnCl_2 \cdot H_2O$ at 2.00 K to much higher fields using a SQUID magnetometer (compliments of Professor Gordon T. Yee), and appear in Figure 11. For fields up to 16 kG isothermal magnetization values here agree well with results from the VSM to within

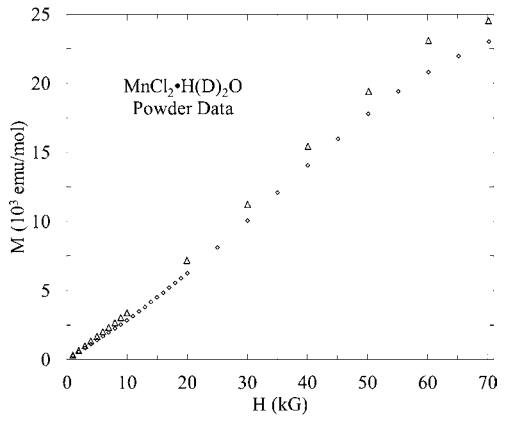

Figure 11. Isothermal molar magnetization vs field at 2.00 K for $MnCl_2 \cdot H_2O$ (diamonds) and $MnCl_2 \cdot D_2O$ (triangles).

dx.doi.org/10.1021/ic4013075 | Inorg. Chem. 2013, 52, 13341−13350

mutual uncertainties. Two features of the data stand out. An inflection appears at an indistinguishable 35(3) kG for each compound. However, the maximum magnetization attained near 7 T is about 6.5% larger for the deuterated compound, 24.5(5) vs 23.0(5) × 10^3 emu/mol. These correspond to 4.39 and 4.12 μ_B/ion, still well below expected saturation near 5 μ_B/ion. The dominant antiferromagnetic intrachain interaction to be overcome by the applied field is weaker in the deuterated compound, hence M obtained at given field and T/T_c is larger.

The standard scenario for a field induced transition in a weakly anisotropic antiferromagnet below its ordering temperature is spin flop. This anisotropy condition can be expected for virtually any Mn(II) compound. For a polycrystalline sample a sharp rise in magnetization at the critical field value H_{SF}, which occurs if measuring along the easy axis, will not appear but rather an inflection appears. Such are clearly present for both compounds in Figure 11, even though T/T_c near 0.9 for 2.00 K is not a small ratio tending to accentuate any anomaly. Mean-field theory yields an expression for the spin flop field at 0 K in terms of effective exchange and anisotropy fields, H_E and H_A, thus[21a]

$$H_{SF}(0) = [2H_E H_A - H_A{}^2]^{\frac{1}{2}} \quad (4)$$

$$H_E = 2z|J|S/g\mu_B \quad (5)$$

$$H_A = 2|D|(S - \frac{1}{2})/g\mu_B \quad (6)$$

where J is the dominant intrasublattice antiferromagnetic exchange integral and where D is the anisotropy constant in the zero-field splitting Hamiltonian already mentioned. Substituting the intrachain exchange interactions already obtained into eq 5, Table 4, yields H_E values 27.9 and 37.3 kG for D_2O and H_2O forms, respectively.

Beyond this point only an approximate evaluation can be made, since H_{SF} at $T/T_c \approx 0.9$ is not a good approximation to the 0 K value. There appear in standard monographs[21a] typical H vs T diagrams for weakly anisotropic antiferromagnets which display a significant reduction in H_{SF} as T decreases. The strength of the variation must be quite system dependent, but a plausible expectation is reduction of H_{SF} by about 30% on going from T/T_c near 1 to 0. Such a reduction needs to be invoked because on employing the observed H_{SF} = 35 kG in eq 4, along with H_E values just given, and solving for H_A, yields (a) only imaginary and hence unphysical values for $MnCl_2{\cdot}D_2O$ and (b) real but unphysically large values for $MnCl_2{\cdot}H_2O$. But using more plausible (if necessarily uncertain) estimates that H_{SF}(0 K) = 25 kG for each compound, now leads to reasonable looking solutions for H_A of 15.5 kG for $MnCl_2{\cdot}D_2O$ and 9.6 kG for $MnCl_2{\cdot}H_2O$. Given the assumptions such estimates are not much more accurate than 20% or so. Substitution into eq 6 yield $|D/k|$ values of 0.5 and 0.3 K for $MnCl_2{\cdot}D_2O$ and $MnCl_2{\cdot}H_2O$, respectively. These are larger than usual for Mn(II) compounds. Nevertheless, the observed susceptibilities should be dominated by exchange interaction effects.

5. DISCUSSION

Very uncommon, probably unique, double chain based structures are reported here for $MnCl_2{\cdot}H_2O$ and $CoCl_2{\cdot}H_2O$. Reorganization of the simpler MCl_2MCl_2M... chains of the dihydrate—also involving two water molecules bonded via oxygen to each metal ion—is driven by the loss of one coordinating ligand and a tendency to attain 6-fold coordination. For the isomorphous dihydrates each of the lattice parameters (monoclinic $C2/m$) is from 2 to 4% smaller on going from $MnCl_2{\cdot}2H_2O$ to $CoCl_2{\cdot}2H_2O$. Just the same range of fractional reductions occur for the (orthorhombic $Pnma$) lattice parameters on passing from $MnCl_2{\cdot}H_2O$ to $CoCl_2{\cdot}H_2O$. A comparable set of local coordination geometry distance reductions occurs from the manganese to the cobalt system, as do distances characterizing interchain hydrogen bonds. The various metal−other atom separations in Table 3 are such that differences between the two compounds average to 0.074 Å, the manganese being larger. This is rather close to the larger ionic radius of Mn(II) relative to Co(II) of 0.08 A.[27a]

This may be refined and extended using accepted ionic radii for the various species involved, with attention to coordination number and spin state.[27b] Values are $r(Cl^-)$ = 1.67 Å for 6-coordination, and similarly $r(O^{2-})$ = 1.26 Å, $r(Mn^{2+})$ = 0.97 Å (high spin), and $r(Co^{2+})$ = 0.885 Å (high spin). Summing these leads to separations Mn−Cl = 2.64 Å, Mn−O = 2.23 Å, Co−Cl = 2.555 Å, and Co−O = 2.145 Å. These are in all cases somewhat larger than the observed values in Table 3, by from 0.04 to 0.14 Å. This is probably attributable to a significant covalent character in all the bonds reported.

An explanation can now be offered based on the structures for the shift from three-dimensional magnetic behavior in dihydrates to quasi-one-dimensional in monohydrates. The smallest metal−metal intrachain separation differs only slightly between dihydrate and monohydrate, despite the reorganization of the chains. These are 3.691 and 3.554 Å in $MnCl_2{\cdot}2H_2O$ and $CoCl_2{\cdot}2H_2O$ respectively, and 3.688 and 3.543 Å in the corresponding monohydrates. The differences of 0.003 and 0.011 Å should yield only rather small changes in the dominant intrachain exchange interaction, still operating via chloride ions bridging the metal ions (see Figures 4 and 5). In the monohydrates there is a next smallest separation between metal ions in different strands of each double chain, which does not exist for the simpler dihydrate chains. These are 3.812 and 3.644 Å in $MnCl_2{\cdot}H_2O$ and $CoCl_2{\cdot}H_2O$, respectively, 0.124 and 0.101 Å larger than the smallest intrachain separations. Because exchange is an extremely strong function of distance it is likely that these separations make much weaker contributions to the overall effective intrachain interaction.

A markedly different situation holds regarding interchain separations. In $MnCl_2{\cdot}2H_2O$ and $CoCl_2{\cdot}2H_2O$ these are 5.752 and 5.616 Å, respectively. In $MnCl_2{\cdot}H_2O$ the two smallest such metal−metal interchain separations are 6.002 and 6.171 Å, while in $CoCl_2{\cdot}H_2O$ they are 5.912 and 6.042 Å. The 0.250 and 0.296 Å minimally larger distances between chains in the monohydrates must certainly weaken interchain exchange substantially, as observed experimentally. Thus the quasi one dimensionality is explained.

However, there is one unexpected finding. A clear difference exists between the detailed appearance of the magnetic susceptibility of $MnCl_2{\cdot}D_2O$ and that of $MnCl_2{\cdot}H_2O$.[1] The 14% lower T_{max} for $MnCl_2{\cdot}D_2O$ than for $MnCl_2{\cdot}H_2O$, and the corresponding smaller magnitude exchange interaction from the Heisenberg model fits, means weaker intrachain ($MnCl_2MnCl_2Mn$...) exchange in deuterated material, though interchain exchange is somewhat larger than in $MnCl_2{\cdot}H_2O$. Hence the deuterated Mn system is a bit less markedly lower dimensional than $MnCl_2{\cdot}H_2O$. But the virtual quantitative identity of the susceptibilities in $CoCl_2{\cdot}H_2O$ and $CoCl_2{\cdot}D_2O$ suggests that no variations in exchange interaction occur between these. The color observations of Sec. 2 now also

appear more significant: no discernible color difference between $CoCl_2·D_2O$ and $CoCl_2·H_2O$, but $MnCl_2·D_2O$ is a gray-violet rather than pink.

Deuteration effects on coordination geometry and ligand field splittings of transition metal complexes involving water are virtually unexamined. Since it is the oxygen of the water which coordinates to the metal ion one expects no significant first order effects. But the coordinated ion with ligands is not isolated. In the present materials interchain hydrogen bonds occur of the type Cl···H−O (relevant Cl−O distances in Table 3; however, neither the H nor D locations can be unambiguously determined from X-ray powder diffraction data). Yet hydrogen bonding is significantly affected by deuteration, because of the smaller vibrational frequency and/or vibrational amplitude of D relative to H; such deuterated bonds are generally weaker.[28]

One attempt to establish a theoretical connection between hydrogen bond strength and superexchange interaction J is especially relevant here because data for several variously hydrated transition metal halides were considered, involving superexchange pathways MA-H··· BM (water oxygen A, with B either a halide or another oxygen).[29] D in place of H tends to be more strongly bonded to A, usually yielding an increased A---B separation. Most important is the contribution of the electrostatic potential energy of the proton, or deuteron, to the covalent component of the A-B bond energy. A significant distinction in an important semiempirical treatment of the hydrogen bond[30] is between so-called "weak" and "strong" cases. For the O−H···O bonds treated this corresponds to an R(O−O) distance ranging from about 2.9 to 2.1 Å. The ionic radius of Cl^- is listed as 0.41 Å larger than that of O;[27b] hence one may estimate the range 3.3 to 2.5 Å for R(O−Cl) in O−H···Cl bonds as from weak to strong. It is known that for strong bonds the change in R(O−O) between H and D forms is positive and from 1 to 2 orders of magnitude larger than for weak bonds, where the corresponding ΔR can be of either sign.[31] It emerges that for strong hydrogen bonds deuteration invariably leads to a decrease in the magnitude of J, of the order 15%.[29] For weak bonds any variation in J is far smaller and can be of either sign, depending on the sign of ΔR, but is usually also a decrease. Most of the compounds analyzed thus[29] were weak bond cases and displayed only quite small changes in J (from a few to less than one percent); an exception was a clearly strong bond case.

The O−Cl distances (Table 3) are well above 3.0 Å and in the weak bond regime; the largest for each compound is too long to constitute a hydrogen bond. Hence deuteration should lead to only quite small changes in J and T_c. For $CoCl_2·H_2O(D_2O)$ this is clearly so. But $MnCl_2·H_2O(D_2O)$ presents puzzling aspects. Because it is a quasi-one-dimensional antiferromagnet T_c is not simply related to a dominant exchange interaction but depends on the values of both J (intrachain) and J' (interchain). Mutual variations of both can be such as not to shift T_c significantly, as reflected in the Table 4 results. However, there is not at hand an explanation for the changes in J and J' on deuteration on the basis of either negligible structural variation or hydrogen bond effect theory.

Nor is there a straightforward explanation for the color change from pink $MnCl_2·H_2O$ to gray-violet $MnCl_2·D_2O$. Gray-violet is in a much shorter wavelength region than pink; hence absorption is dominated by (color complement) longer wavelength(s), or smaller frequencies. This implies a decrease in the crystal field splitting on deuteration, in a quite distorted pseudo-octahedral geometry where the situation can be rather different from that of a low lying set of t_{2g} orbitals and a pair of excited e_g orbitals. There is a somewhat wider range of Mn−Cl separations in Table 3 than Co−Cl separations. The coordination geometry of the $MnCl_5O$ moieties is slightly more distorted than for $CoCl_5O$. This is also the case for the dihydrate compounds.[32] We have found (unpublished) that $MnCl_2·2D_2O$ is also gray-violet, in contrast to pink $MnCl_2·2H_2O$, but that the magnetic susceptibilities of these two compounds are virtually indistinguishable. This is definitely in contrast to the situation for $MnCl_2·H_2O$ and $MnCl_2·D_2O$.

The observed colors of complexes are not necessarily easily interpretable in the above straightforward way when two or more comparable absorption features occur in the visible or near visible. The optical spectroscopy of the present systems is beyond the scope of this paper. It seems that the identity of the metal ion as Mn(II) is significant. But it is difficult to see why a single presumably stronger bond (O−D) in a $MnCl_5O$ coordination sphere should yield a significant reduction in (effective) crystal field splitting, with no such effect in $CoCl_5O$.

■ ASSOCIATED CONTENT

Ⓢ Supporting Information

X-ray crystallographic details in CIF format. This material is available free of charge via the Internet at http://pubs.acs.org.

■ AUTHOR INFORMATION

Corresponding Authors

*E-mail: spagol@wm.edu.
*E-mail: gxdefo@wm.edu.

Notes

The authors declare no competing financial interest.

■ ACKNOWLEDGMENTS

S.P. gratefully acknowledges time to collect synchrotron diffraction data at beamline X16C, N.S.L.S., Brookhaven National Laboratory, supported by the Office of Basic Energy Sciences of the DOE under contract No. DE-AC02-98CH10886. G.C.D. gratefully acknowledges grants from the Solid State Chemistry Program, DMR-NSF and from the Donors of the American Chemical Society Petroleum Research Fund. He has also benefitted from a Plumeri Faculty Award at the College of William and Mary.

■ REFERENCES

(1) DeFotis, G. C.; Wiese, R. S.; Scherrer, C. W. *J. Appl. Phys.* **1990**, *67*, 5857.
(2) Lukin, J. A.; Friedberg, S. A.; DeFotis, G. C. *J. Appl. Phys.* **1991**, *69*, 5807.
(3) DeFotis, G. C.; Chamberlain, R. V.; Jarvis, W. R. A.; Krovich, D. J. *J. Magn. Magn. Mater.* **1992**, *104−107*, 1603.
(4) Lukin, J. A.; Friedberg, S. A.; Chandarlapaty, S.; Brubaker, W. W.; Cinquina, C. C.; DeFotis, G. C. *J. Appl. Phys.* **1994**, *75*, 5529.
(5) DeFotis, G. C.; Coffey, G. A.; Cinquina, C. C.; Charndarlapaty, S.; Brubaker, W. W.; Krovich, D. J.; Chamberlain, R. V.; Jarvis, W. R. A. *Phys. Rev.* **1995**, *B51*, 15113.
(6) McElearney, J. N.; Merchant, S.; Carlin, R. L. *Inorg. Chem.* **1973**, *12*, 906 and references therein.
(7) Moore, J. E.; Butera, R. A. *J. Solid State Chem.* **1986**, *61*, 263.
(8) Narath, A. *Phys. Rev.* **1964**, *136*, A766; *Phys. Rev.* **1965**, *140*, A552 and references therein.
(9) Boultif, A.; Louer, D. *J. Appl. Crystallogr.* **2004**, *37*, 724.
(10) Werner, P. E.; Eriksson, L.; Westdahl, M. *J. Appl. Crystallogr.* **1985**, *18*, 367.

(11) Le Bail, A. *Powder Diffr.* **2005**, *20*, 316.
(12) Rodríguez Carvajal, J. *Phys. B* **1993**, *192*, 55.
(13) *International Tables for Crystallography*, 5th ed.; Hahn, T., Ed; Springer: New York, 2005; Vol. *A*, Space-group symmetry.
(14) Altomare, A.; Caliandro, R.; Camalli, M.; Cuocci, C.; Giacovazzo, C.; Moliterni, A. G. G.; Rizzi, R. *J. Appl. Crystallogr.* **2004**, *37*, 1025.
(15) (a) Rietveld, H. M. *J. Appl. Crystallogr.* **1969**, *2*, 65. (b) Young, R. A., Ed.; *The Rietveld Method*; Oxford Univ. Press: New York, 2002.
(16) Larson, A. C.; Dreele, R. B. *General Structure Analysis System (GSAS)*; Los Alamos Laboratory Report No. LA-UR-86-748; Los Alamos National Laboratory: Los Alamos, NM, 2004.
(17) Thompson, P.; Cox, D. E.; Hastings, J. B. *J. Appl. Crystallogr.* **1987**, *20*, 79.
(18) Finger, L. W.; Cox, D. E.; Jephcoat, A. P. *J. Appl. Crystallogr.* **1994**, *27*, 892.
(19) Scott, H. G. *J. Appl. Crystallogr.* **1983**, *16*, 159.
(20) DeFotis, G. C.; Wallo, C. D.; Smith, R. L.; Bodkin, D. B.; Mirabilio, G. L.; Leftwich, T. R.; Kim, M. G.; Reed, Z. D. *Phys. Rev.* **2005**, *B71*, 224415.
(21) (a) Carlin, R. *Magnetochemistry*; Springer-Verlag: New York, 1986. (b) Stout, J. W.; Hadley, W. B. *J. Chem. Phys.* **1964**, *40*, 55.
(22) König, E.; Kremer, S. *Magnetism Diagrams for Transition Metal Ions*; Plenum Press: New York, 1979.
(23) Smith, T.; Friedberg, S. A. *Phys. Rev.* **1968**, *176*, 660.
(24) Oguchi, T. *Phys. Rev.* **1964**, *133*, A1098.
(25) Hennessy, M. J.; McElwee, C. D.; Richards, P. M. *Phys. Rev.* **1973**, *B7*, 930.
(26) Richards, P. M. *Phys. Rev.* **1974**, *B10*, 4687.
(27) (a) Sharpe, A. G. *Inorganic Chemistry*; Longman: London, U.K., 1986. (b) Shannon, R. D. *Acta Crystallogr.* **1976**, *A32*, 751.
(28) Lutz, H. D. *Struct. Bonding (Berlin)* **1988**, *69*, 97.
(29) Turrell, B. G.; Yue, C. L. *Can. J. Phys.* **1969**, *47*, 2575.
(30) Reid, C. *J. Chem. Phys.* **1959**, *30*, 182.
(31) Ubbelohde, A. R.; Gallagher, K. J. *Acta Crystallogr.* **1955**, *8*, 71.
(32) Morosin, B.; Graeber, E. J. *Acta Crystallogr.* **1963**, *16*, 1176; *J. Chem. Phys.* **1965**, *42*, 898.